# High Aperture Efficiency Wide Corrugations Bull's-Eye Antenna working at 60 GHz

Unai Beaskoetxea and Miguel Beruete

***Abstract*—A full metallic Bull's-Eye (BE) antenna operating at 60 GHz is numerically and experimentally analyzed. The antenna presents wide grooves, rather than narrow ones, which support higher order resonances that lead to a large gain enhancement with just a pair of corrugations, achieving an overall miniaturization and increase of its aperture efficiency. In addition, an annular soft surface of 5 grooves is placed on the edge of the antenna, giving rise to a slight increase of the gain, reduced side lobe level as well as reduced end-fire and backward radiation, when compared with an antenna without soft surface and another antenna with narrow corrugations. A narrow beam antenna with a gain of 19 dBi and nearly –16 dB side lobe level and 10.8 deg beamwidth is numerically obtained at the operating frequency. Measurements and numerical results show overall good agreement, with an experimental gain of 20.2 dBi, –13.2 dB side lobe level, 10.4 deg beamwidth and 32% of aperture efficiency.**

***Index Terms*— bull's eye antenna, high aperture efficiency, miniaturized, soft surface, wide corrugations.**

## I. Introduction

Bull's-Eye (BE) topology has attracted a lot of interest in the last few years due to its interesting features, especially in the field of antennas, such as a high-gain and narrow beamwidth in an all-metallic and low profile geometry. The most common geometry of BE antennas consists in a central radiating aperture surrounded by annular concentric grooves. They were developed more than a decade ago in the microwave range from the basis of extraordinary transmission structures [1]–[3], and have been further explained in terms of leaky waves [4]–[6]. Nowadays, BE are considered as a new family of antennas [7], [8], that can be a practical alternative to horns or even reflector antennas in applications where a reduced profile is needed [9], [10] and that are compatible with the most advanced production technologies such as additive manufacturing techniques (3D-printed stereolithography) [11] or even planar structures printed on low-cost substrates [12]–[15]. Another niche where BE antennas are finding a remarkable relevance is the terahertz (THz) band [16]–[18]. A common drawback of BE antennas is their relatively low aperture efficiency, given that they are structures with several periods (typically 6 or more) with a periodicity near the operation wavelength. For example, the BE in [8] has an aperture efficiency of $e_a$ = 6.25%, the design of [9] has $e_a$ = 1.61% and that of [10] has $e_a$ = 4.2%. A way to improve the radiation characteristics is to reduce the radiation at the borders. This can be accomplished by adding a soft surface (SS) [19]–[21], i.e., a short period grating that prevents the currents from reaching the edge of the structure, as was done by Huang *et al*. in [22]. With this strategy, the aperture efficiency was increased to $e_a$ ~ 13.32%.

A remarkable increase of the gain and aperture efficiency can be achieved with wide corrugations, as demonstrated in [23], due to the excitation of the Transverse Magnetic $TM_{11}$ mode inside the wide corrugations instead of the Transverse Electric $TE_{11}$ mode, which is the only mode supported by narrow grooves (this modal analysis considers the grooves as coaxial waveguides). It is worth remarking that the BE in [8] was halfway between a narrow and a wide corrugations antenna and therefore the gain obtained was not maximum.

In this work, we present a BE antenna fed by a resonating slot working at 60 GHz which takes advantage of the use of wider corrugations, with the addition of a concentric SS to get a much higher gain and lower side lobe level compared to an antenna with narrow and no SS. Thus, a very high aperture efficiency (considering the whole disc diameter, i.e. both wide corrugations and soft surface) of $e_a$ = 32% is obtained. Numerical and experimental analysis are carried out, showing good agreement between simulation and measurement results.

## II. Prototype Design and Simulations

The wide corrugation Bull's Eye with SS (WBESS) antenna considered in this paper is shown in Fig. 1(a). It consists of a metallic plane with a central slot surrounded by a pair of concentric annular wide grooves and by an external set of five narrow grooves, all of them designed to operate at 60 GHz.

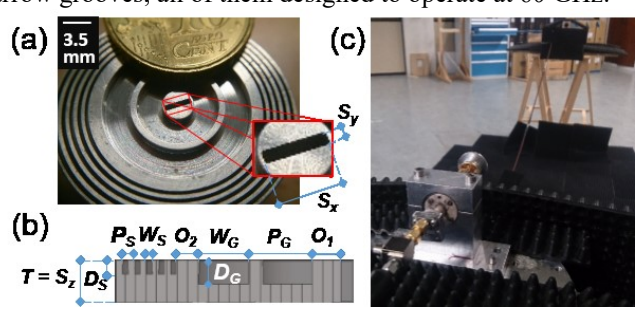


Fig. 1. (a) Photograph showing the fabricated WBESS antenna. (b) Cross-sectional view schematic. (c) Experimental setup.

The numerical analyses in this paper are done using the Transient Solver included in the commercial software CST Microwave Studio™ [24] in the frequency range from 50 GHz to 70 GHz (with a step of 200 MHz). The antenna is made of a lossy metal with conductivity σ = 1.856 × $10^7$ S/m, as in the experiment. The geometry is mapped using a non-uniform hexahedral mesh with smallest mesh cell of 61 μm × 61 μm × 109 μm (0.012λ × 0.012λ × 0.022λ). In order to reduce computational burden, electric and magnetic symmetries are used for the *x-z* plane and the *y-z* plane, respectively. The

This paper was submitted for review on xxxxxxxxxx
U. Beaskoetxea, and M. Beruete are with the Antennas Group-TERALAB, Universidad Pública de Navarra, Pamplona, 31006, Spain (e-mail: unai.beaskoetxea@unavarra.es; miguel.beruete@unavarra.es). M. Beruete is also with the Institute of Smart Cities, Public University of Navarra.
This work was supported by the Spanish Ministerio de Economía y Competitividad (MINECO) under contract TEC2014-51902-C2-2-R.
M.B. acknowledges support by the Spanish Ministerio de Economía y Competitividad (MINECO) under contract RYC-2011-08221. U.B acknowledges the funding provided by UPNA via the FPI PhD grant program.

antenna is fed by a WR-15 standard waveguide (V-band) attached to the rear part. The supplied power is coupled to the free space by means of a resonating slot. As an initial value, the slot's width ($S_x$) and depth ($S_z$) are set to λ/2 and the slot's height ($S_y$) is set to λ/8 with λ = 5 mm for $f$ = 60 GHz. To design the wide grooves (placed at an initial distance from the slot in the $y$ direction $O_1$ = 1.45 mm), the initial values were taken from [23] as a seed (scaled in frequency) and then refined by means of an optimization routine (based on the Trust Region Framework algorithm provided by CST). The final dimensions returned by the optimization process are shown in Table I.

TABLE I
WBESS DIMENSIONS

| Parameter | Description | Initial Values (mm / λ**) | Optim. Values (mm / λ**) |
|---|---|---|---|
| $Sx$ | Slot Width | 2.50 / 0.50 | 3.54 / 0.71 |
| $Sy$ | Slot Height | 0.62/ 0.12 | 0.75 / 0.15 |
| $Sz$ | Slot Depth | 2.50 / 0.50 | 2.50 / 0.50 |
| $W_G$ | Wide Groove Width | 3.54 / 0.71 | 3.12 / 0.62 |
| $D_G$ | Wide Groove Depth | 0.85 / 0.17 | 1.42 / 0.28 |
| $P_G$ | Wide Groove Period | 4.25 / 0.85 | 3.94 / 0.79 |
| $W_S$ | SS* Groove Width | 0.31 / 0.06 | 0.36 / 0.07 |
| $D_S$ | SS* Groove Depth | 1.25 / 0.25 | 0.82 / 0.16 |
| $P_S$ | SS* Groove Period | 0.62 / 0.12 | 0.74 / 0.15 |
| $O_1$ | Offset Distance 1 | 1.45 / 0.29 | 2.08 / 0.42 |
| $O_2$ | Offset Distance 2 | 2.50 / 0.50 | 1.36 / 0.27 |

*SS makes reference to Soft surface
**λ = 5mm at $f$ = 60 GHz

Regarding the SS, according to [19], [20], the initial values can be calculated as $P_s - W_s << P_s << \lambda/2$ and $D_s = \lambda/4$ where $P_s$ is the period of the grating, $W_s$ and $D_s$ are, respectively, the width and the depth of the grooves. To find the final values, an optimization routine (using the same algorithm and considering the number of grooves and their width, depth and period) was carried out setting as goal achieving the lowest possible side lobe levels. The initial and final values are shown in Table I. Obviously, the final dimensions deviate from the initial values, which are only valid strictly for a structure with infinite periods. In our case, we have a relatively short structure and, in addition, there is some interaction between the SS and the adjacent corrugations. Moreover, another important parameter is the distance between the start of the SS and the last groove of the WBE, $O_2$, which must be such that the minimum side lobe level value is obtained at the frequency of design. An optimization of this parameter with seed $O_2 = d/2$ was done. Table I summarizes all the WBESS dimensions.

For comparison purposes a narrow corrugations BE (NBE) and a third structure, identical to the WBESS but with no soft surface (WBE), were also analyzed. The NBE designed for this purpose has a central resonant slot with dimensions 2.5 mm × 0.48 mm and is surrounded by three concentric annular corrugations with $W_G$ = 0.64 mm and $D_G$ = 1.04 mm distributed with a period $P_G$ = 4.98 mm in a metallic disc of diameter Ø 24 mm and thickness of 1.1 mm. We opted for three narrow corrugations instead of two in order to obtain a structure comparable in size to the wide corrugations antennas.

Fig. 2 shows the broadband simulation results for the three structures, comprising the reflection coefficient (a) gain (b), and the E-plane (c) and H-plane (d) radiation diagrams at $f$ ~ 60 GHz. The antennas with wide corrugations present two dips in the reflection coefficient response [dotted red and dash-dotted black curves, Fig. 2(a)], corresponding the one at $f_1$ ~ 60 GHz to the cavity resonance of the wide corrugations (fixed by their dimensions) and the one at $f_2$ ~ 65 GHz to the longitudinal resonance of the slot (λ/2 ~ $S_z$). The transversal resonance corresponding to the slot's width is located at $f$ = 43 GHz (λ/2 ~ $S_x$), out of the frequency span shown in the figure.

Note that although the WBESS presents an impedance matching bandwidth of 10 GHz (from 58.8 GHz to 68.8 GHz, where the $S_{11}$ is below −10 dB), only 2 GHz (fixed by the 3 dB gain bandwidth) is of interest for the application. As for the NBE antenna (dashed blue curves), it displays a single dip corresponding to the transversal resonance of the slot in the range of interest, whereas the longitudinal resonance is shifted to higher frequencies.

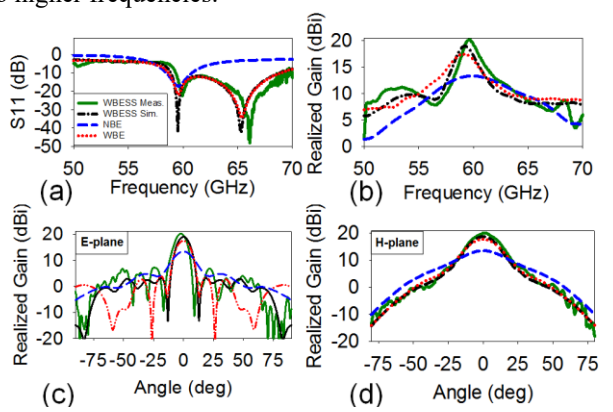


Fig. 2. Simulation results for WBESS (dash-dotted black), WBE (dotted red) and NBE (dashed blue) and experimental results for WBESS (solid green). (a) S11 magnitude in dB and (b) realized gain in dBi as a function of frequency and radiation diagrams for (c) E-plane and (d) H-plane at 60 GHz.

As it is well known, a closed waveguide resonator (a cavity) has its resonant frequency fixed by its depth, width and height dimensions [25]. An open ended waveguide (slot) and the wide corrugations present a similar behavior. Although the width of the slot fixes the transversal resonance frequency and the depth fixes the longitudinal resonance, the modification of any of them directly implies a modification of the slot cavity, resulting in the observed shifting of the resonances in Fig. 3. Thus, a narrower [$x$ direction, Fig. 3(c)] or shorter [$z$ direction, Fig. 3(d)] slot results in a dip located at a higher frequency (dotted curve), while a wider [Fig. 3(c)] or longer [Fig. 3(d)] slot locates it (dashed curves) below the optimized slot resonance (solid curves). However, the variation of the slot's width has no effect on the grooves' resonance, Fig. 3(c), unlike the slot's length, Fig. 3(d), which affects the Q factor of the resonance at ~ $f$ = 60 GHz.

It is observed that a variation of the groove's width or depth leads to a shift in the frequency of the first plotted dip (grooves' resonance), as it can be observed in Figs. 3(a, b). A narrower or shallower groove with respect to the optimized dimension (continuous curve) results in a shift towards higher

frequencies (dotted curves), while the converse shifts the dip towards lower frequencies (dashed curves). In a similar way, the grooves' dimensions affect the longitudinal resonance, Figs. 3(a, b), fixing, for example, the minimum disc thickness and, consequently, the maximum frequency of the longitudinal resonance dip. This is the reason why, to obtain impedance matching at a certain frequency, both the slot and the surrounding corrugations (and the offset distance from the center of the slot at which the corrugation grating is placed) must be analyzed simultaneously.

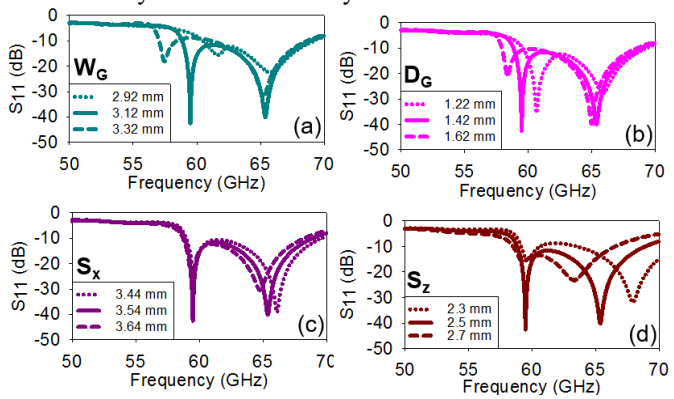


Fig. 3. Numerical study of the $S_{11}$ magnitude *vs* the variation of several parameters: (a) groove's width and (b) depth; (c) slot´s width and (d) length.

As shown in Figs. 2(b-d), despite having 3 corrugations, the NBE presents at the operating frequency (60 GHz) the lowest gain of all the designs (13.3 dBi), the highest side lobe level (−8.7 dB) and the largest beamwidth ($\theta_{-3dB}$ = 18 deg). The wide corrugations antennas show, at approximately $f$ = 60 GHz, a gain enhancement of more than 4 dB for the WBE (17.5 dBi) and nearly +6 dB for the WBESS (19 dBi). In addition, lower side lobe levels (−13.8 dB and −16 dB) and narrower beamwidths (12 deg and 10.8 deg) are obtained for the WBE and WBESS, respectively.

It is interesting to observe the beaming behavior of this antenna at frequencies other than design. For this, four radiation patterns have been obtained (two for E- and *x-z* middle-plane at 55 GHz and 65 GHz), see Fig. 4. For frequencies below $f$ = 60 GHz, the E-plane shows two beams [Fig. 4(a)] which tend to broadside as frequency is swept towards the frequency of design. In contrast, for frequencies above $f$ = 60 GHz, the single beam reduces its gain and becomes a near isotropic beam [Fig. 4(c)] as frequency is swept towards higher frequencies. As for the *x-z* middle-plane, it presents a near isotropic low gain beam at frequencies below and above the frequency of design [Fig. 4(b, d)].

Evidently, as the structure presents a magnetic symmetry in the *y-z* plane (corresponding to the E-plane) and an electric symmetry in the *x-z* plane (corresponding to the H-plane at the design frequency), both planes display a null of cross-polar. However, it is interesting to note that the measured cross-polarization shows values lower than 7dB from -90 to 90 deg for the plane cut at 42 deg (which displays the largest cross-polar values), as it can be observed in Fig. 4(e).

It is also important to stress that, although the WBESS is approximately 1.2 times larger than the analyzed NBE and the WBE, it would be necessary to design a NBE threefold larger than the current WBESS to achieve the same gain (with an estimated calculation of +1dB for each narrow corrugation). Nevertheless, the radiation enhancement achieved in the E-plane by using wide corrugations comes along with an increase of the backward and end-fire radiation, as it can be seen for the WBE in Fig. 2(c). The inclusion of the soft surface minimizes drastically the end-fire radiation (19.2 dB lower value) and backward radiation (3dB less power radiated in the back half-semisphere) contributing also to a slight increase of the gain (+1.5 dB) as well as a reduction of the side lobe level (1.9 dB lower value). The inclusion of the soft surface minimizes drastically the end-fire radiation and decreases the backward radiation. This can be appreciated in Fig. 5, where the fields scattered at the edge of the structure for both no SS (a) and SS (b) cases are displayed. The SS must be properly optimized since the use of incorrect groove dimensions would lead to a deterioration of the radiated beam, with an increase of the side lobe level and a decrease of the gain.

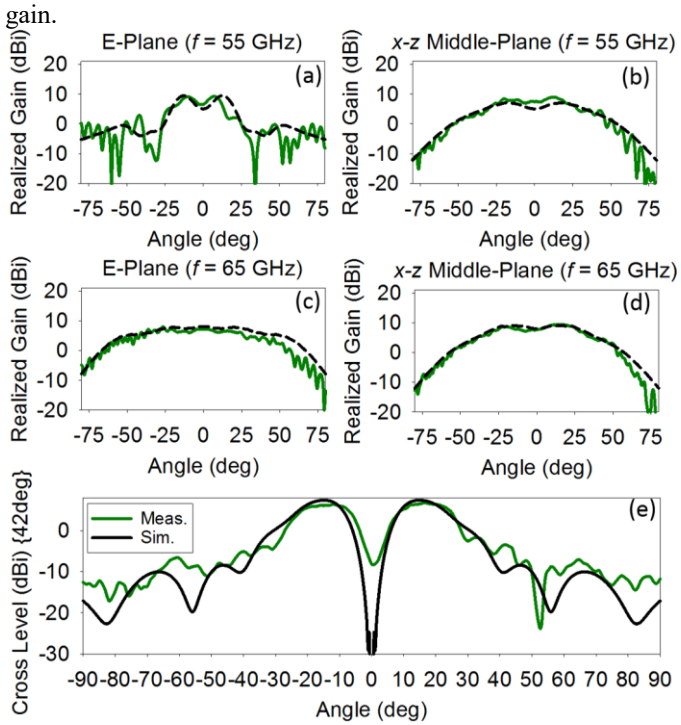


Fig. 4. Simulated (black curves) and experimental (green curves) radiation diagrams at frequencies other than $f$ = 60 GHz. E- and *x-z* middle-plane at (a, b) $f$ = 55 GHz and (c, d) at $f$ = 65 GHz. (e) Cross-Polar for a plane cut at 42 deg and $f$ = 60GHz.

The insertion of even more corrugations would lead to a higher gain and narrower beam as demonstrated in the inset of Fig. 6, increasing almost up to 24.4 dBi for the 8-period structure (solid green line). However, this deteriorates the aperture efficiency, as displayed in Fig. 6, where it can be observed that the efficiency drops down to 19% for 8 corrugations (note that increasing $P$ implies also an increase of the aperture size). Note also that the aperture efficiencies displayed in Fig. 7 correspond to numerical results and that the $e_a$ = 32 % mentioned in the introduction corresponds to the experimental results presented in the next section).

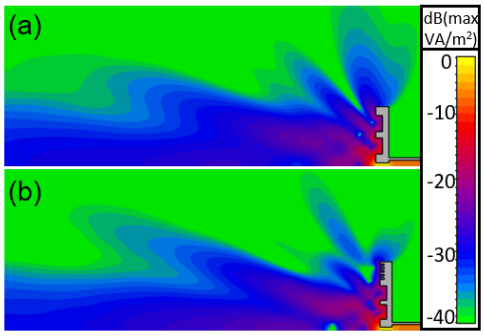


Fig. 5. Power Flow profile of (a) WBE and (b) WBESS.

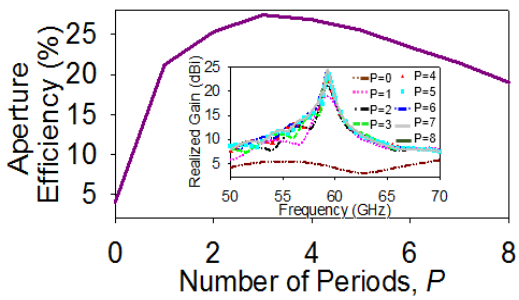


Fig. 6. Simulated aperture efficiency for an increasing number $P$ of wide corrugation periods at the operation frequency. (Inset) Realized gain as a function of frequency as $P$ is varied.

The fields inside the grooves are analyzed for both the NBE and the WBESS antenna to find the dominant mode in each case, following the approach of [23]. At the design frequency, the narrow groove, Fig. 7(a), supports a $TE_{11}$ mode as demonstrated by its coaxial waveguide counterpart (designed with identical dimensions). In contrast, the field distribution inside the WBESS antenna grooves, Fig. 7(b), is dominated by the $TM_{11}$ mode (which, due to the symmetries imposed by the excitation, is the first higher order mode inside a coaxial waveguide). According to [23], the excitation of the $TM_{11}$ mode leads to an enhancement of the transmission and a higher gain.

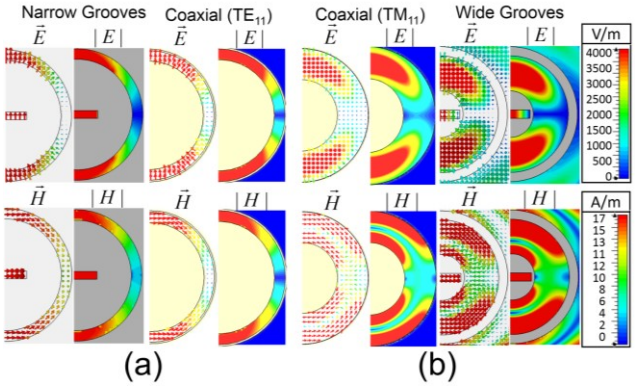


Fig. 7. (a) Field distribution inside the NBE antenna compared with the fundamental $TE_{11}$ mode of a coaxial waveguide at $f$ = 59.25 GHz. (b) Idem for a WBESS antenna compared with the $TM_{11}$ mode of a coaxial waveguide.

## III. Prototype Fabrication and Measurements

The previously discussed WBESS was manufactured and measured. Although the design with 3 corrugations has an aperture efficiency $e_a$ = 27.4% larger than the case of 2 corrugations ($e_a$ = 25.3%), we selected the latter to get a compact and miniaturized structure. The raw material used for the manufacturing was EN AW-7075 (AlZn5.5MgCu), with electric conductivity $\sigma \sim 1.856 \times 10^7$ S/m. First, a section of this material underwent a turning process to machine the outside geometry, followed by a milling process to machine holes and threads. Then the structure went through a spark erosion process, where corrugations and the central slot were obtained by means of die erosion. A photograph of the fabricated prototype is shown in Fig. 1(a).

The experimental characterization of the antenna was done by means of an ABmm™ Vector Network Analyzer (VNA) equipped with a software controllable rotary platform. To avoid spurious reflections, nearby surfaces (walls, tables, platform, cables…) as well as the path between antennas, were covered with millimeter-wave absorbers (setup shown in Fig. 1(c)). The return loss was obtained in the range of 50 GHz to 70 GHz with a step of 50 MHz, by following a two-step calibration process. First, the output of a WR-15 waveguide directional coupler, attached to an isolator (which, in turn, is directly fed by the VNA by means of a coaxial cable attached to a Schottky diode – i.e. frequency multiplier – and an attenuator), was short-circuited by a plane metallic mirror, to obtain the maximum reflection. Then, the antenna was attached to the directional coupler pointing towards an open area and the reflected power was recorded. The measured reflection coefficient is displayed with a solid green line in Fig. 2(a). It is below −10 dB from 59.35 GHz to 69 GHz, although the operational bandwidth is 2.78% around the working frequency, defined by the 3 dB gain bandwidth, in good agreement with the numerical simulation.

The antenna broadband gain and radiation patterns were obtained by applying the gain-transfer (gain comparison) method [26]. First, two identical standard V-band horn antennas of known gain were placed face to face at a distance of 6 m (being 3.13 m and 4.9 m the farfield distances for the WBESS antenna and the horn antennas, respectively, at $f$ = 60 GHz), 1.10 m above the floor and 1.5 m below the ceiling and the free-space transmission was obtained. Then, the test antenna was replaced by the WBESS mounted on the rotary platform. To measure the E- and H-plane radiation diagrams, the WBESS was rotated from −90 to +90 deg (step of 0.5 deg), and measured from 50 to 70 GHz (step of 50 MHz).

Fig. 2(b) shows the recorded broadband gain. Near 60 GHz, the antenna shows a gain peak, both in the simulation and experimental results. It reaches a level of 20.2 dBi in the experiment, 1.2 dB higher than in the simulation, probably due to the constructive interference of spurious reflections in the experimental setup. This gain implies a high aperture efficiency $e_a$ = 32% (compared with previous designs of the corrugated BE family). Solid green curves in Figs. 2(c) and (d) display the simulated and experimental E- and H-plane radiation diagrams, respectively. Radiation patterns at $f$ = 55 GHz and 65 GHz are shown in Fig. 4. It can be seen in Fig. 2(c) that the side lobe level in the experiment is 2.6 dB higher than in the simulation results (−13.2 dB) probably due to unwanted reflections in the experimental facilities. However,

the beamwidth presents a similar minimum value (11.5 deg for the simulation and 10.4 deg for the measured antenna). With regard to the cross-polarization level, values below 7 dBi (which corresponds to the highest value) are observed for the whole measured frequency range (see Fig. 5). In general, numerical and measurement results show good agreement.

## IV. Conclusions

A miniaturized BE antenna, consisting of a resonant slot surrounded by 2 wide corrugations and a SS of 5 narrow corrugations, has been designed, fabricated and measured. The utilization of wide corrugations permits the excitation of the higher-order mode $TM_{11}$ inside the grooves, which leads to a large gain enhancement. Thus, a compact structure whose radiation characteristics surpass those of an antenna with narrow corrugations (which excite the fundamental mode $TE_{11}$) is obtained. Including a SS drastically reduces end-fire and backward radiation, as it prevents the currents from reaching the edges and back part of the structure. Simulation results show that the use of wide corrugations and SS provides +6dB gain (19 dBi) and a reduction of near 8 dB (−16 dB) and ~ 8 deg (10.8 deg) for the side lobe level and beamwidth, respectively, when compared with a BE with narrow corrugations and no SS. Simulation results and measurements for the WBESS present an overall good agreement, with a gain of 20.2 dBi, a side lobe level of −13.2 dB and a beamwidth of $\theta_{-3dB}$ = 10.4 deg. It is noteworthy that, due to its reduced size and high gain, this antenna presents an aperture efficiency noticeably larger than other structures of the corrugated BE family ($e_a$ = 32%). This kind of geometry can be of high interest in applications like secure short range point-to-point communications where the optimal utilization of the usually limited available space is essential, in 5G communications or for the emerging deployment of the 60 GHz license free wireless communications.

## References

[1] H. J. Lezec, A. Degiron, E. Devaux, R. A. Linke, L. Martin-Moreno, F. J. Garcia-Vidal, and T. W. Ebbesen, "Beaming light from a subwavelength aperture," *Science*, vol. 297, no. 5582, pp. 820–822, Aug. 2002.

[2] M. Beruete, M. Sorolla, I. Campillo, J. S. Dolado, L. Martín-Moreno, J. Bravo-Abad, and F. J. García-Vidal, "Enhanced millimeter-wave transmission through subwavelength hole arrays.," *Opt. Lett.*, vol. 29, no. 21, pp. 2500–2502, Nov. 2004.

[3] M. Beruete, I. Campillo, J. S. Dolado, J. E. Rodríguez-Seco, E. Perea, and M. Sorolla, "Enhanced microwave transmission using a subwavelength slot in corrugated plate," *IEEE Antennas Propag. Soc. AP-S Int. Symp.*, vol. 3 A, no. 1, pp. 14–17, Dec. 2005.

[4] A. A. Oliner and D. R. Jackson, "Leaky-Wave Antennas," in *Antenna Engineering Handbook*, J. L. Volakis, Ed. New York: Mc Graw-Hill, 2007, pp. 11-1-56.

[5] D. R. Jackson, A. A. Oliner, T. Zhao, and J. T. T. Williams, "Beaming of light at broadside through a subwavelength hole: Leaky wave model and open stopband effect," *Radio Sci.*, vol. 40, no. 6, pp. 1–12, Dec. 2005.

[6] D. R. Jackson, P. Burghignoli, G. Lovat, F. Capolino, J. Chen, D. R. Wilton, and A. A. Oliner, "The Fundamental Physics of Directive Beaming at Microwave and Optical Frequencies and the Role of Leaky Waves," *Proc. IEEE*, vol. 99, no. 10, pp. 1780–1805, 2011.

[7] M. Beruete, I. Campillo, J. S. Dolado, E. Perea, F. Falcone, and M. Sorolla, "Dual-band low-profile corrugated feeder antenna," *IEEE Trans. Antennas Propag.*, vol. 54, no. 2, pp. 340–350, 2006.

[8] M. Beruete, I. Campillo, J. S. Dolado, J. E. Rodríguez-Seco, E. Perea, F. Falcone, and M. Sorolla, "Very Low-Profile 'Bull's Eye' Feeder Antenna," *IEEE Antennas Wirel. Propag. Lett.*, vol. 4, no. 2, pp. 365–368, 2005.

[9] C. J. Vourch and T. D. Drysdale, "V-Band 'Bull's Eye' Antenna for CubeSat Applications," *IEEE Antennas Wirel. Propag. Lett.*, vol. 13, pp. 1092–1095, 2014.

[10] U. Beaskoetxea, V. Pacheco-Peña, B. Orazbayev, T. Akalin, S. Maci, M. Navarro-Cía, and M. Beruete, "77 GHz High Gain Bull's-Eye Antenna With Sinusoidal Profile," *IEEE Antennas Wirel. Propag. Lett.*, vol. 14, pp. 205–208, 2015.

[11] U. Beaskoetxea, S. Maci, M. Navarro-Cía, and M. Beruete, "3D-Printed 96 GHz Bull's-Eye Antenna with Off-Axis Beaming," *IEEE Trans. Antennas Propag.*, vol. 65, no. 1, pp. 17–25, 2017.

[12] P. Baccarelli, P. Burghignoli, G. Lovat, and S. Paulotto, "A novel printed leaky-wave 'bull-eye' antenna with suppressed surface-wave excitation," in *IEEE Antennas and Propagation Society Symposium, 2004.*, 2004, vol. 1, pp. 1078–1081.

[13] S. K. Podilchak, P. Baccarelli, P. Burghignoli, A. P. Freundorfer, and Y. M. M. Antar, "Optimization of a Planar 'Bull-Eye' Leaky-Wave Antenna Fed by a Printed Surface-Wave Source," *IEEE Antennas Wirel. Propag. Lett.*, vol. 12, pp. 665–669, 2013.

[14] S. K. Podilchak, P. Baccarelli, P. Burghignoli, A. P. Freundorfer, and Y. M. M. Antar, "Analysis and Design of Annular Microstrip-Based Planar Periodic Leaky-Wave Antennas," *IEEE Trans. Antennas Propag.*, vol. 62, no. 6, pp. 2978–2991, 2014.

[15] S. K. Podilchak, Y. M. M. Antar, A. Freundorfer, P. Baccarelli, P. Burghignoli, S. Paulotto, and G. Lovat, "Planar antenna for continuous beam scanning and broadside radiation by selective surface wave suppression," *Electron. Lett.*, vol. 46, no. 9, p. 613, 2010.

[16] N. Yu, R. Blanchard, J. Fan, Q. J. Wang, C. Pflügl, L. Diehl, T. Edamura, S. Furuta, M. Yamanishi, H. Kan, and F. Capasso, "Plasmonics for Laser Beam Shaping," *IEEE Trans. Nanotechnol.*, vol. 9, no. 1, pp. 11–29, 2010.

[17] N. Yu, Q. J. Wang, M. A. Kats, J. A. Fan, S. P. Khanna, L. Li, A. G. Davies, E. H. Linfield, and F. Capasso, "Designer spoof surface plasmon structures collimate terahertz laser beams.," *Nat. Mater.*, vol. 9, no. 9, pp. 730–735, Sep. 2010.

[18] M. Beruete, U. Beaskoetxea, M. Zehar, A. Agrawal, S. Liu, K. Blary, A. Chahadih, X.-L. Han, M. Navarro-Cía, D. Etayo, A. Nahata, T. Akalin, and M. Sorolla, "Terahertz Corrugated and Bull's-Eye Antennas," *IEEE Trans. Terahertz Sci. Technol.*, vol. 3, no. 6, pp. 740–747, Nov. 2013.

[19] P.-S. Kildal, "Artificially soft and hard surfaces in electromagnetics," *IEEE Trans. Antennas Propag.*, vol. 38, no. 10, pp. 1537–1544, 1990.

[20] P.-S. Kildal, "Artificially soft and hard surfaces in electromagnetics and their application to antenna design," in *23rd European Microwave Conference, 1993*, 1993, pp. 30–33.

[21] R. Quarfoth and D. Sievenpiper, "Alteration of electromagnetic scattering using hard and soft anisotropic impedance surfaces," *IEEE Trans. Antennas Propag.*, vol. 63, no. 10, pp. 4593–4599, 2015.

[22] C. Huang, Z. Zhao, and X. Luo, "Application of 'bull's eye' corrugated grooves integrated with artificially soft surfaces structure in the patch antenna to improve radiation performance," *Microw. Opt. Technol. Lett.*, vol. 51, no. 7, pp. 1676–1679, Jul. 2009.

[23] D. Yeop, K.-Y. Jung, and Y. Bae, "Transmission Through an Annular Aperture Surrounded With Corrugations in a PEC Plane," *Antennas Wirel. Propag. Lett. IEEE*, vol. 14, pp. 179–182, 2015.

[24] www.cst.com, "CST Microwave Studio." .

[25] David M. Pozar, *Microwave Engineering Fourth Edition*. John Wiley & Sons, 2005.

[26] "IEEE Standard Test Procedures for Antennas," *ANSI/IEEE Stand. 149-1979*, 1979.